

Measurement of the Higgs boson branching ratio $\text{BR}(H \rightarrow \gamma\gamma)$ at a 3 TeV CLIC

G. Kačarević^{✉,*}, I. Božović-Jelisavčić[✉], N. Vukašinović[✉], G. Milutinović-Dumbelović,
I. Smiljanić[✉], and T. Agatonović-Jovin

“VINČA” Institute of Nuclear Sciences—National Institute of the Republic of Serbia,
University of Belgrade, 11000 Belgrade, Serbia

M. Radulović[✉] and J. Stevanović[✉]

University of Kragujevac, Faculty of Science, 34000 Kragujevac, Serbia



(Received 11 January 2022; accepted 28 January 2022; published 20 May 2022)

In this paper we address the potential of a 3 TeV center-of-mass energy Compact Linear Collider (CLIC) to measure the branching fraction of the Higgs boson decay to two photons, $\text{BR}(H \rightarrow \gamma\gamma)$. Since photons are massless, the Higgs boson coupling to photons is realized through higher order processes involving heavy particles either from the Standard Model or beyond. Any deviation of the measured $\text{BR}(H \rightarrow \gamma\gamma)$, and consequently of the Higgs coupling $g_{H\gamma\gamma}$ from the predictions of the Standard Model, may indicate new physics. The Higgs decay to two photons is thus an interesting probe of the Higgs sector. This study is performed using the simulation of the detector for CLIC and by considering all relevant physics and beam-induced processes in a full reconstruction chain. It is shown that the product of the Higgs production cross section in W^+W^- fusion and $\text{BR}(H \rightarrow \gamma\gamma)$ can be measured with a relative statistical uncertainty of 5.5%, assuming the integrated luminosity of 5 ab^{-1} and unpolarized beams.

DOI: [10.1103/PhysRevD.105.092009](https://doi.org/10.1103/PhysRevD.105.092009)

I. INTRODUCTION

The Higgs boson decay to a pair of photons was one of the discovery channels at the LHC [1,2] and also a benchmark process that has shaped requirements for the electromagnetic calorimetry at ATLAS [3] and CMS [4]. This channel is also important at proposed e^+e^- colliders, both in terms of detector performance requirements and complementary to the expected HL-LHC results [5]. Global fit of data collected through a staged realization of a linear collider as a Higgs factory leads to a relative statistical uncertainties of the Higgs to photons coupling ($g_{h\gamma\gamma}$) at the level of 1–2% [6]. In particular, operation at the highest center-of-mass energy improves statistical precision due to vector boson-fusion modes of the Higgs boson production. This uncertainty is an order of magnitude smaller than the one achievable with the current LHC data [7]. Accuracy of the $g_{h\gamma\gamma}$ determination at the future electron-positron colliders is comparable to the one of the combined ATLAS and CMS projection for HL-LHC of 1.8% for the total relative uncertainty [6]. However, the combined HL-LHC and future e^+e^- collider measurements are expected to give sub percent accuracy of the Higgs to photons coupling [6].

CLIC provides an excellent environment to study the properties of the Higgs boson, including its couplings, with a very high precision. Operation is expected to be staged at three center-of-mass energies: at 380 GeV, 1.5 TeV, and 3 TeV. WW fusion, t-channel exchange of W bosons, (Fig. 1) as the dominant Higgs production mechanism at center-of-mass energies above ~ 500 GeV will produce large signal yields allowing rare processes such as $H \rightarrow \mu^+\mu^-$, $H \rightarrow Z\gamma$ and $H \rightarrow \gamma\gamma$ to be studied. As can be seen from the Fig. 1, Higgs boson coupling to photons is realized through higher order processes that may involve heavy, beyond the Standard Model physics. Thus Higgs boson diphoton decay is an interesting process to probe eventual realization of beyond the Standard Model physics in the Higgs sector. Typically, $g_{h\gamma\gamma}$ could be modified up to 1–3% in the most sensitive cases [8], requiring a combination of individual measurements, like the one presented in this paper through a global fit of data within a single experiment or even combinations between experiments, in particular with HL-LHC. For a Higgs mass of 126 GeV, the SM prediction for the branching fraction $\text{BR}(H \rightarrow \gamma\gamma)$ is 2.23×10^{-3} [9]. It is expected that 2×10^6 Higgs bosons will be produced at 3 TeV, assuming the nominal integrated luminosity of 5 ab^{-1} which will be used in this paper unless stated otherwise. The signal yield can be increased with the proposed beam polarization by a factor of 1.5 [10]. The high photon-identification efficiency and good photon

*kacarevicgoran@vin.bg.ac.rs

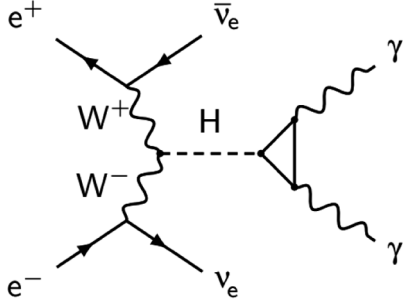


FIG. 1. Lowest order Feynman diagram of the Higgs production in WW fusion and subsequent Higgs decay to a pair of photons.

energy resolution of a detector for CLIC enable excellent identification of $H \rightarrow \gamma\gamma$ decays.

This paper presents a comprehensive simulation of the experimental measurement of the Higgs production cross section in WW fusion $\sigma(e^+e^- \rightarrow H\nu\bar{\nu}) \times \text{BR}(H \rightarrow \gamma\gamma)$ at 3 TeV CLIC. The result of the study presented here supersedes the estimates based on 1.4 TeV studies given in [11]. The paper is structured as follows: simulation and analysis tools are introduced in Sec. II, the detector for CLIC is described in Sec. III, while Secs. IV–VI provide details on signal and background identification and separation, pseudoexperiments and uncertainties of the measurement.

II. SIMULATION AND ANALYSIS TOOLS

The Higgs production in WW fusion is generated in WHIZARD 1.95 [12], where a Higgs mass of 126 GeV is assumed. Background processes are also generated in WHIZARD, using PYTHIA 6.4 [13] to simulate hadronization and fragmentation processes. The CLIC luminosity spectrum and beam-induced effects are obtained using GuineaPig 1.4.4 [14]. Interactions with the detector are simulated using the CLIC_ILD detector model [15] within the MOKKA simulation package [16] based on the GEANT4 framework [17]. Events are reconstructed using the particle flow approach (PFA) implemented in the Pandora algorithm [18]. Photons are reconstructed with PandoraPFA v02-04-00 photon processor [19]. Simulation, reconstruction and analysis are carried out using ILC DIRAC [20]. The TMVA package [21] is employed for the multivariate analysis classification (MVA) of signal and background events on the basis of their kinematic properties.

III. DETECTOR FOR CLIC

The CLIC_ILD model is based on the ILD detector proposed for ILC [22] and it has been modified to the CLIC experimental conditions. The vertex detector is closest to the interaction point to provide reconstruction of secondary vertices for accurate flavor tagging. The time projection chamber is foreseen as the main tracking device providing

single point resolution better than $100 \mu\text{m}$ in the plane transverse to the beam axis [15], together with a low material budget. The CLIC_ILD detector uses high-granularity electromagnetic (ECAL) and hadronic sampling calorimeters to reconstruct photons and neutral hadrons. The electromagnetic calorimeter is a silicon-tungsten calorimeter optimized for longitudinal containment and lateral separation of electromagnetic showers. High granularity in combination with the information from the central tracker leads to an electron identification efficiency of 96%, while photon identification efficiency is 99% [23]. The hadronic calorimeter consists of 60 steel absorbers interleaved with scintillator tiles to contain hadronic showers from neutral hadrons [15]. A more recent detector model CLICdet [24] improves the stochastic energy resolution term of the ECAL to 17% from 20% of CLIC_ILD. This, however has no significant impact on the conclusions of this paper.

IV. SIGNAL AND BACKGROUND PROCESSES

The main Higgs production processes and backgrounds considered in this paper are summarized in Fig. 2 and Table I. Signal events are generated as $e^+e^- \rightarrow \nu\bar{\nu}H \rightarrow \nu\bar{\nu}\gamma\gamma$ events, but, at the reconstruction level, they include particles (particle flow objects) that could be realistically present in the detector, from hadrons produced by Beamstrahlung in $\gamma_{BS}\gamma_{BS} \rightarrow$ hadrons, including final state radiation of these states, to the Beamstrahlung photons themselves. Thus the number of the reconstructed photons per signal event is significantly larger than two (in average around 140) and calls for the preselection methods to identify the Higgs candidate that is a diphoton system truly originating from the Higgs boson decay. Background processes are considered as simultaneously present with the signal in 5 ab^{-1} of data in the amounts indicated in Table I. Each background process is simulated under the same assumptions of realistic experimental conditions as for the signal, including initial state radiation and final state radiation, realistic luminosity spectrum, presence of Beamstrahlung photons and hadrons produced by

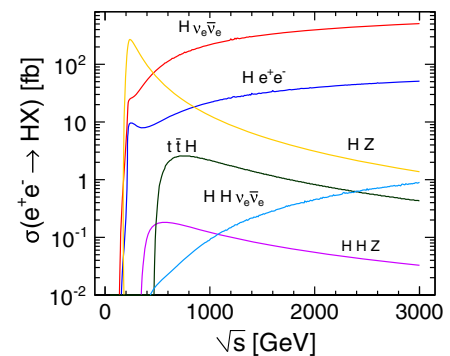


FIG. 2. Higgs production cross sections at different center-of-mass energies.

TABLE I. Signal and background processes with the corresponding effective^a cross sections at 3 TeV center-of-mass energy.

Signal process	$\sigma(fb)$	N@5 ab ⁻¹	N _{simulated}
$e^+e^- \rightarrow H\nu\nu, H \rightarrow \gamma\gamma$	0.95	4750	24550
Background processes	$\sigma(fb)$	N@5 ab ⁻¹	N _{simulated}
$e^+e^- \rightarrow \gamma\gamma$	15.2	7.6×10^4	3×10^4
$e^+e^- \rightarrow e^+e^-\gamma$	335	1.7×10^6	3×10^6
$e^+e^- \rightarrow e^+e^-\gamma\gamma$	33	1.6×10^5	1.5×10^5
$e^+e^- \rightarrow \nu\bar{\nu}\gamma$	13	6.6×10^4	2×10^5
$e^+e^- \rightarrow \nu\bar{\nu}\gamma\gamma$	26	1.3×10^5	1.6×10^5
$e^+e^- \rightarrow q\bar{q}\gamma$	210	1.1×10^6	1.2×10^6
$e^+e^- \rightarrow q\bar{q}\gamma\gamma$	47	2.3×10^5	3×10^5

^aThe cross sections are effective in a sense that condition $100 \text{ GeV} < m_{\gamma\gamma} < 150 \text{ GeV}$ is applied to any diphoton system found in the central tracker.

Beamstrahlung overlaid in each event before the digitization phase.

Higgs boson production at 3 TeV is dominated by the WW fusion process. Without beam polarization, the effective cross section for the Higgs production is 415 fb, including initial state radiation effects as well as a realistic CLIC luminosity spectrum. Taking into account that $\text{BR}(H \rightarrow \gamma\gamma)$ is order of 0.23%, 4750 signal events are expected with the nominal integrated luminosity. In order to describe fully the CLIC experimental environment, simulated Beamstrahlung photons producing hadrons ($\gamma_{BS}\gamma_{BS} \rightarrow \text{hadrons}$) are overlaid on each event after the full simulation of the detector response and before the digitization phase. Background processes are considered if two generated photons can be found in the central tracker acceptance with the invariant mass of diphoton system between 100 and 150 GeV. Backgrounds arising from monophoton final states are considered as well if an auxiliary photon (from $\gamma_{BS}\gamma_{BS} \rightarrow \text{hadrons}$ overlay, final state radiation or false particle identification) can be found in the detector polar angle acceptance, forming an invariant mass with the final-state photon that falls in the selected window.

V. EVENT SELECTION

A. Photon isolation and Higgs candidate definition

To ensure that Higgs candidates are found, only events with exactly two isolated photons with transverse momenta greater than 15 GeV are selected. The requirement that both photons have p_T above 15 GeV removes to a great extent reconstructed photons in a signal event that do not originate from the Higgs decays, as illustrated in Fig. 3. We define a photon isolated if the energy of all reconstructed particles, except photon, within a 14 mrad cone is less than 20 GeV. This isolation criterion reduces background processes (in particular $e^+e^- \rightarrow q\bar{q}\gamma$ and $e^+e^- \rightarrow q\bar{q}\gamma\gamma$) by 23%. Signal

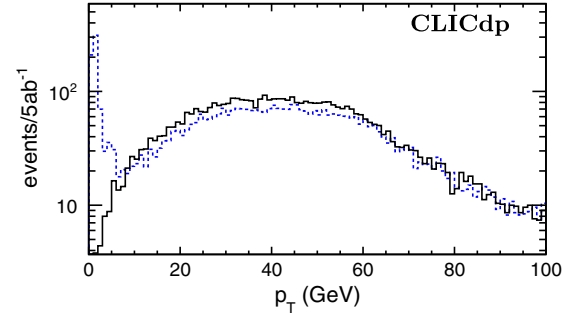


FIG. 3. The second highest reconstructed photon p_T in a signal event (dashed) and the second highest p_T of a generated photon originating from a Higgs decay (solid). The difference in the two distributions at low p_T values comes from the presence of Beamstrahlung photons in signal events at the reconstructed level (dashed).

loss is negligible. Selection of events with exactly two isolated photons with $p_T > 15 \text{ GeV}$ results in 22.3% signal loss, as illustrated in Fig. 4.

B. Preselection

Signal is separated from backgrounds in a two-stage selection process: preselection and MVA based selection. The preselection suppresses high cross section backgrounds like $e^+e^- \rightarrow e^+e^-\gamma$ and $e^+e^- \rightarrow e^+e^-\gamma\gamma$. Preselection variables are optimized as follows:

- (1) Reconstructed diphoton invariant mass in the range from 110 to 140 GeV, corresponding to the Higgs mass window.
- (2) Reconstructed diphoton energy in the range between 100 and 1000 GeV.
- (3) Reconstructed diphoton transverse momentum in the range between 20 and 600 GeV.

Distributions of diphoton energy and transverse momentum are given in Figs. 5(a) and 5(b), respectively, illustrating the choice of selection range. The signal and background diphoton invariant mass after preselection is given in Fig. 6. Preselection efficiency for signal is 70% and background dominates over the signal by a factor of 25.

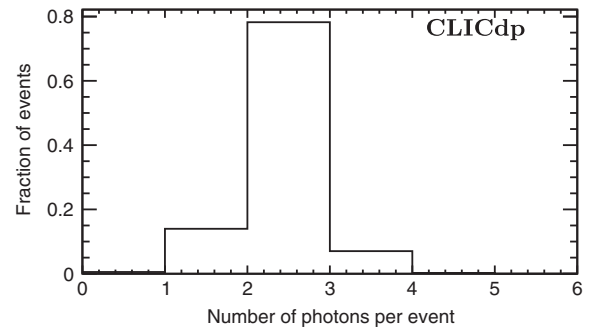


FIG. 4. Number of reconstructed isolated photons per signal event with $p_T(\gamma) > 15 \text{ GeV}$.

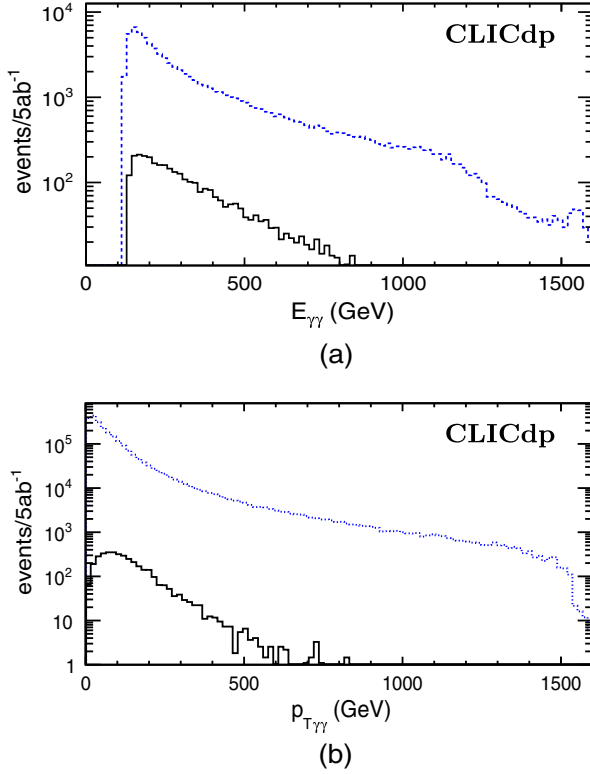


FIG. 5. Higgs candidate observables for signal and overall background from Table I: energy (a) and transverse momentum (b). Signal is represented with the solid line while background is represented as dashed.

C. Multivariate analysis

Preselected signal and background events are further separated using an MVA method based on the gradient boosted decision trees (BDTG). Twelve observables are used for classification of events: diphoton energy, diphoton transverse momentum, diphoton polar angle, cosine of the helicity angle, transverse momenta of photons, polar angle

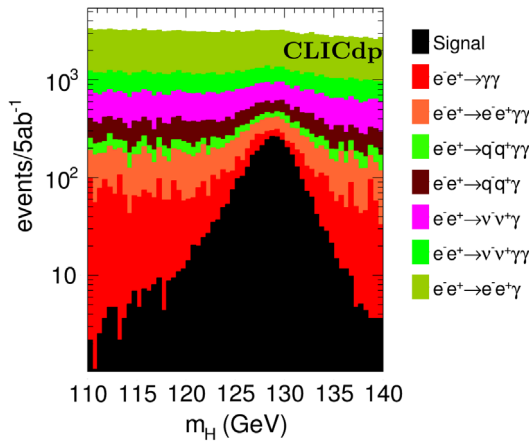


FIG. 6. Stacked histograms of Higgs mass distributions for signal and background after preselection.

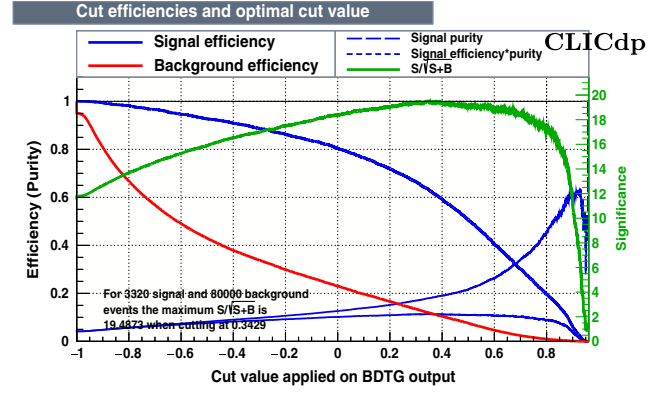


FIG. 7. BDTG performance in the training phase.

of photons, energy of photons, total ECAL energy per event and total hadronic sampling calorimeter energy per event. The optimal cut-off value of the BDTG output variable was found to be 0.34, as illustrated in Fig. 7. Variables are sufficiently uncorrelated for MVA to perform optimally.

The classifier cut was selected to maximize statistical significance defined as

$$S = \frac{N_s}{\sqrt{N_s + N_b}}, \quad (1)$$

where N_s and N_b are the number of signal and background events after the MVA selection. The MVA efficiency for signal is 62.7%, resulting in an overall signal selection efficiency of 43.7%, corresponding to a signal yield of 2080 selected Higgs candidates. The remaining background after the MVA application is ~ 10 times larger than the signal and originates mostly from the processes such as $e^+e^- \rightarrow \nu\bar{\nu}\gamma$ and $e^+e^- \rightarrow \nu\bar{\nu}\gamma\gamma$ or from a high cross section process like $e^+e^- \rightarrow e^+e^-\gamma$. The Higgs candidate mass distribution after MVA selection is illustrated in Fig. 8, giving the composition of the background.

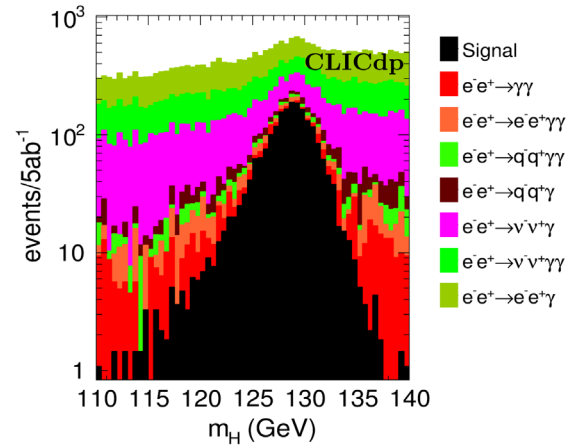


FIG. 8. Stacked histograms of Higgs mass distributions for signal and background after MVA selection.

VI. PSEUDOEXPERIMENTS

A. Method

The observable to be measured is a product of the Higgs production cross section and a corresponding branching fraction for Higgs diphoton decay and it can be experimentally determined from the counted number of signal events N_s as

$$\sigma(e^+e^- \rightarrow H\nu\bar{\nu}) \times \text{BR}(H \rightarrow \gamma\gamma) = \frac{N_s}{L \cdot \epsilon_s}, \quad (2)$$

where L represents the integrated luminosity, and ϵ_s is the overall signal efficiency including detector acceptance, photon identification efficiency and signal selection efficiency. The number of signal events will be determined from combined fit of diphoton invariant mass distributions of selected simulated (or experimental) data with the function f :

$$f(m_{\gamma\gamma}) = N_s \cdot f_s(m_{\gamma\gamma}) + N_b \cdot f_b(m_{\gamma\gamma}), \quad (3)$$

where N_s and N_b are the number of selected signal and background events, and f_s and f_b are the probability density functions (PDFs) describing $m_{\gamma\gamma}$ for signal and background, respectively. These PDFs are determined from simulated samples of signal and background data.

B. Signal and background PDF

Functions f_s and f_b from Eq. (3) are used to fit the fully simulated datasets of signal and background after the MVA selection phase. The signal PDF consists of two Gaussian functions, one describing the tail (f_{flat}) and the other describing exponential part (f_{exp}) of diphoton mass distribution of the signal:

$$f_s = f_{\text{flat}} + C_1 \cdot f_{\text{exp}},$$

$$f_{\text{flat}} = \begin{cases} e^{-\frac{(m_{\gamma\gamma}-m_H)^2}{2\sigma^2+\beta_L(m_{\gamma\gamma}-m_H)^2}} & (m_{\gamma\gamma} < m_H), \\ e^{-\frac{(m_{\gamma\gamma}-m_H)^2}{2\sigma^2+\beta_R(m_{\gamma\gamma}-m_H)^2}} & (m_{\gamma\gamma} > m_H), \end{cases}$$

$$f_{\text{exp}} = \begin{cases} e^{-\frac{(m_{\gamma\gamma}-m_H)^2}{2\sigma^2+\alpha_L|m_{\gamma\gamma}-m_H|}} & (m_{\gamma\gamma} < m_H), \\ e^{-\frac{(m_{\gamma\gamma}-m_H)^2}{2\sigma^2+\alpha_R|m_{\gamma\gamma}-m_H|}} & (m_{\gamma\gamma} > m_H), \end{cases} \quad (4)$$

where σ , C_1 , $\alpha_{L,R}$, $\beta_{L,R}$ as well as Higgs mass m_H are free parameters determined by the fit (Fig. 9). The fit is performed using ROOFIT [25].

The diphoton mass distribution for background is fitted with a linear function f_b :

$$f_b = p_0 + p_1 \cdot m_{\gamma\gamma}, \quad (5)$$

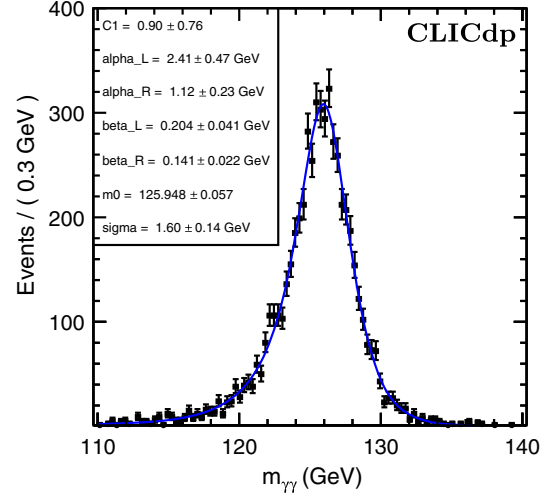


FIG. 9. Fit of diphoton invariant mass of the selected signal (points) and the fit function f_s (line).

where p_0 and p_1 are free parameters of the fit. The fit of background diphoton invariant mass distribution is illustrated in Fig. 10, and shows no sensitivity to the SM Higgs mass.

C. Pseudoexperiments

The pseudodata distribution, combining both signal and background after MVA selection, is fitted with function f [Eq. (3)], where N_s and N_b are set as free parameters. In this way the number of signal events is determined in the same way it would be on a set of experimental data. Such a measurement we call a pseudoexperiment. An example of one pseudoexperiment is shown in Fig. 11. In order to estimate the statistical dissipation of the measured number of signal events, 5000 pseudoexperiments with 5 ab^{-1} of data were performed. Pseudodata for signal is randomly picked from fully simulated signal sample, while $m_{\gamma\gamma}$

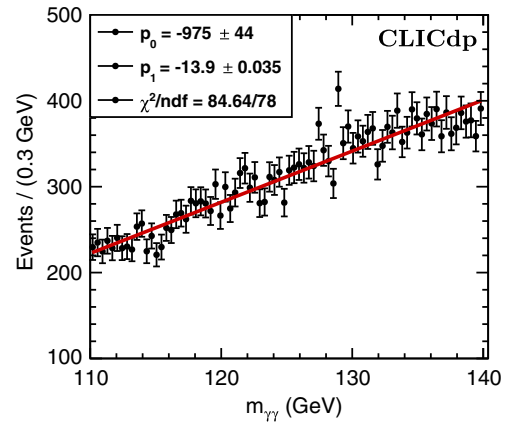


FIG. 10. Diphoton invariant mass $m_{\gamma\gamma}$ for the sum of all background processes remaining after event selection (points). The fit function given in Eq. (5) is overlaid (line).

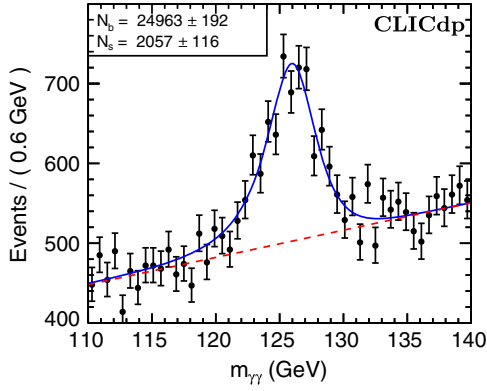


FIG. 11. Example of one pseudoexperiment, showing diphoton invariant mass of pseudodata (black), corresponding fit with the function f from Eq. (3) (full line) and background fit with function f_b (dashed line) from Eq. (5).

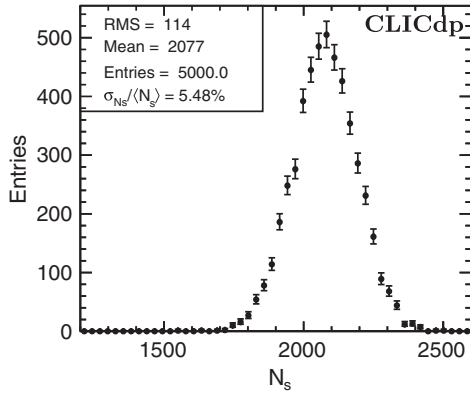


FIG. 12. Pull distribution of 5000 pseudoexperiments.

distribution for background is generated from background PDF by randomly changing parameters p_0 and p_1 from Eq. (5). The rms of the resulting pull distribution over all pseudoexperiments is taken as the estimate of the statistical uncertainty of the measurement (Fig. 12). It reads that the statistical uncertainty of the extracted number of signal events is 5.5%.

D. Systematic uncertainty

Several sources of systematic uncertainty of the measurement are considered. The systematic uncertainty associated with photon identification requires more detailed investigation as it depends on the distribution of material and details of the treatment of converted photons within the particle flow algorithm. As converted photons account for of order 10% of all photons, the overall systematic uncertainty from this source is expected to be smaller than the statistical uncertainty. Assuming for illustration an uncertainty on the photon identification efficiency of 0.5%, it would result in a systematic uncertainty of about 1% on the $\text{BR}(H \rightarrow \gamma\gamma)$ measurement. The relative

uncertainty of the integrated luminosity, and hence of the measured cross section, is expected to be of order of several per mill at CLIC [26]. Another source of systematic uncertainty is due to the uncertainty of the luminosity spectrum reconstruction. In [27] it has been shown that the CLIC luminosity spectrum at 3 TeV center-of-mass energy can be corrected better than 5% above 50% of the nominal center-of-mass energy, while above 75% of the nominal center-of-mass energy the corresponding uncertainty of the correction is at a per mill level [28]. As discussed in [11], the impact of uncertainty of the luminosity spectrum reconstruction on $H\nu\bar{\nu}$ production at 3 TeV (in $H \rightarrow b\bar{b}$ channel) is found to be of order of several per mill. The energy resolution of the ECAL also has the per-mill-level impact on preselection efficiency. If we assume the relative uncertainty of the ECAL sampling term of 10%,¹ then the resulting uncertainty of reconstructed photon energy of ~ 40 MeV has a negligible effect on N_s determination. Similarly, the uncertainty of diphoton transverse momentum as a preselection variable hardly contributes to the systematic uncertainty of the measurement. To probe the systematic sensitivity of the result to background modeling, linear fit from the Eq. (5) was replaced with the second order polynomial function. Negligible (per mill) level impact is found. With the considerations above, relative systematic uncertainty of the measurement is expected to be smaller than the statistical one.

VII. SUMMARY

The accessibility of WW fusion as a dominant Higgs production mechanism at energies of 500 GeV and above enable the Higgs rare decays at 3 TeV CLIC to be measured. Excellent performance of the electromagnetic calorimeter to identify high-energy photons together with the overall PFA reconstruction of physics processes enables the measurement of the loop induced Higgs decays to two photons at the percent level. In the full simulation of experimental measurement, we have shown that $\sigma(e^+e^- \rightarrow H\nu\bar{\nu}) \times \text{BR}(H \rightarrow \gamma\gamma)$ can be measured at 3 TeV CLIC with a relative statistical uncertainty of 5.5%, assuming 5 ab^{-1} of integrated luminosity and unpolarized beams. This result can be further improved with the proposed beam polarization scheme, which would increase the Higgs production cross section by a factor of 1.5, due to the chiral nature of WW fusion as a charged-current interaction. The systematic uncertainty of this measurement is estimated to be smaller than the statistical one. This analysis completes the set of Higgs to measurements foreseen at CLIC energy stages above 1 TeV center-of-mass energy.

¹As shown in [29,30] ECAL can be usually calibrated with the relative uncertainty of the sampling term $\sim 10\%$.

ACKNOWLEDGMENTS

The work presented in this paper has been carried out in the framework of the CLIC detector and physics study (CLICdp) collaboration and the authors would like to thank the CLICdp members for their support. We are in particular grateful to the colleagues from the Analysis Working Group for useful discussions, to Philipp Roloff,

for useful ideas exchanged in the course of the analysis and to Aleksander Filip Zarnecki who contributed to the paper by raising several important questions. Our special thanks goes to Nigel Watson for editing the text. This research was supported by the Science Fund of the Republic of Serbia, Grant No. 7699827, HIGHTONE-P.

-
- [1] ATLAS Collaboration, Observation of a new particle in the search for the Standard Model Higgs boson with the ATLAS detector at the LHC, *Phys. Lett. B* **716**, 1 (2012).
- [2] CMS Collaboration, Observation of a new boson at a mass of 125 GeV with the CMS experiment at the LHC, *Phys. Lett. B* **716**, 30 (2012).
- [3] J. Colas *et al.*, Response uniformity of the ATLAS liquid argon electromagnetic calorimeter, *Nucl. Instrum. Methods Phys. Res., Sect. A* **582**, 429 (2007).
- [4] The CMS Collaboration *et al.*, Electron and photon reconstruction and identification with the CMS experiment at the CERN LHC, *J. Instrum.* **16**, P05014 (2021).
- [5] M. Cepeda, S. Gori, P. Ilten, M. Kado, F. Riva *et al.*, Higgs physics at the HL-LHC and HE-LHC, Report No. CERN-LPCC-2018-04, 2019.
- [6] Mara Cepeda (on behalf of the Higgs@Future Colliders working group), Higgs precision measurements at future colliders, CERN Council Open Symposium on the Update of European Strategy for Particle Physics, Report No. C19-05-13.2, Granada, 2019.
- [7] CMS Collaboration, Combined Higgs boson production and decay measurements with up to 137 fb¹ of proton-proton collision data at $\sqrt{s} = 13$ TeV, Report No. CMS PAS HIG-19-005.
- [8] Fujii, Keisuke *et al.*, Physics case for the 250 GeV stage of the international linear collider, [arXiv:1710.07621v4](https://arxiv.org/abs/1710.07621v4).
- [9] S. Dittmaier *et al.*, *Handbook of LHC Higgs cross sections: 2. Differential distributions* (CERN, Geneva, 2012), p. 275, [10.5170/CERN-2012-002](https://arxiv.org/abs/10.5170/CERN-2012-002).
- [10] H. Abramowicz, N. Alipour Tehrani, D. Arominski *et al.*, Top-quark physics at the CLIC electron-positron linear collider, *J. High Energy Phys.* **11** (2019) 003.
- [11] H. Abramowicz, A. Abusleme, K. Afanaciev *et al.*, Higgs physics at the CLIC electron-positron linear collider, *Eur. Phys. J. C* **77**, 475 (2017).
- [12] W. Kilian, T. Ohl, and J. Reuter, WHIZARD: Simulating multi-particle processes at LHC and ILC, *Eur. Phys. J. C* **71**, 1742 (2011).
- [13] T. Sjostrand, S. Mrenna, and P.Z. Skands, PYTHIA 6.4 physics and manual, *J. High Energy Phys.* **05** (2006) 026.
- [14] D. Schulte, Beam-beam simulations with GUINEA-PIG, Report No. CERN-PS-99-014-LP, 1999.
- [15] L. Linssen *et al.*, Physics and detectors at CLIC: CLIC conceptual design report, Reports No. ANL-HEP-TR-12-01, No. CERN-2012-003, No. DESY 12-008, KEK Report 2011–2017.
- [16] P. Mora de Freitas and H. Videau, Detector simulation with MOKKA/GEANT4: Present and future, International Workshop on Linear Colliders, Report No. LC-TOOL-2003-010, JeJu Island, Korea, 2002.
- [17] S. Agostinelli *et al.*, Geant4—a simulation toolkit, *Nucl. Instrum. Methods Phys. Res., Sect. A* **506**, 250 (2003).
- [18] J. S. Marshall, A. Mnnich, and M. Thomson, Performance of particle flow calorimetry at CLIC, *Nucl. Instrum. Methods Phys. Res., Sect. A* **700**, 153 (2013).
- [19] F. Gaede, Marlin and LCCD: Software tools for the ILC, *Nucl. Instrum. Methods Phys. Res., Sect. A* **559**, 177 (2006).
- [20] C. Grefe, S. Poss, and A. Sailer, ILCDIRAC, a DIRAC extension for the linear collider community, Report No. CLICdp-Conf 2013-003, CERN, Geneva, 2013.
- [21] A. Hocker *et al.*, TMVA—Toolkit for multivariate data analysis, [arXiv:physics/0703039](https://arxiv.org/abs/physics/0703039).
- [22] T. Abe *et al.*, The international large detector: Letter of intent, [10.2172/975166](https://arxiv.org/abs/10.2172/975166) (2010).
- [23] D. Arominski *et al.*, A detector for CLIC: Main parameters and performance, [arXiv:1812.07337v1](https://arxiv.org/abs/1812.07337v1).
- [24] CLICdp Collaboration, CLICdet: The post-CDR CLIC detector model, Report No. CLICdp-Note-2017-001, 2017.
- [25] W. Verkerke and D. P. Kirkby, The RooFit toolkit for data modeling, eConf **C03033241**, MOLT007 (2003).
- [26] I. Bozovic-Jelisavcic, S. Lukic, G. Milutinovic Dumbelovic, M. Pandurovic, and I. Smiljanic, Luminosity measurement at ILC, *J. Instrum.* **8**, P08012 (2013).
- [27] S. Poss and A. Sailer, Luminosity spectrum reconstruction at linear colliders, *Eur. Phys. J. C* **74**, 2833 (2014).
- [28] S. Lukic, I. Bozovic-Jelisavcic, M. Pandurovic, and I. Smiljanic, Correction of beam-beam effects in luminosity measurement in the forward region at CLIC, *J. Instrum.* **8**, P05008 (2013).
- [29] CMS Collaboration, Energy calibration and resolution of the CMS electromagnetic calorimeter in pp collisions at $\sqrt{s} = 7$ TeV, *J. Instrum.* **8**, P09009 (2013).
- [30] I. Smiljanic, Method of luminosity measurement at the international linear collider, Ph.D thesis, University of Belgrade, 2016.